Nonlinear Analysis: Modelling and Control, 2009, Vol. 14, No. 1, 85–102

# Computational Modelling of Biosensors with an Outer Perforated Membrane*

**K. Petrauskas**[1], **R. Baronas**[1,2]

[1]Department of Software Engineering, Vilnius University
Naugarduko str. 24, LT-03225 Vilnius, Lithuania
k.petrauskas@gmail.com

[2]Institute of Mathematics and Informatics
Akademijos str. 4, LT-08663 Vilnius, Lithuania

**Received:** 2008-12-21 **Revised:** 2009-03-02 **Published online:** 2009-03-10

**Abstract.** This paper presents one-dimensional (1-D) and two-dimensional (2-D) in-space mathematical models for amperometric biosensors with an outer perforated membrane. The biosensor action was modelled by reaction-diffusion equations with a nonlinear term representing the Michaelis-Menten kinetics of an enzymatic reaction. The conditions at which the 1-D model can be applied to simulate the biosensor response accurately were investigated numerically. The accuracy of the biosensor response simulated by using 1-D model was evaluated by the response simulated with the corresponding 2-D model. A procedure for a numerical evaluation of the effective diffusion coefficient to be used in 1-D model was proposed. The numerically calculated effective diffusion coefficient was compared with the corresponding coefficients derived analytically. The numerical simulation was carried out using the finite difference technique.

**Keywords:** biosensor, perforated membrane, modelling, numerical simulation.

## 1 Introduction

Biosensors are analytical devices made up of a combination of a specific biological element, usually an enzyme, that recognizes a specific analyte (substrate) and the transducer that translates the biorecognition event into an electrical signal [1, 2]. The amperometric biosensors measure the current that arises on a working electrode by direct electrochemical oxidation or reduction of the biochemical reaction product. The current is proportional to the concentration of the target analyte.

The biosensors are widely used in clinical diagnostics, environment monitoring, food analysis and drug detection because they are reliable, highly sensitive and relatively cheap

*This work was partially supported by Lithuanian State Science and Studies Foundation, project No. N-08007.

devices [3–5]. However, amperometric biosensors possess a number of serious drawbacks. One of the main reasons restricting wider use of the biosensors is a relatively short linear range of the calibration curve [6]. Another serious drawback is the instability of bio-molecules. These problems can be partially solved by an application of an additional outer perforated membrane [1–3].

To improve the productivity and efficiency of a biosensor design as well as to optimize the biosensor configuration a model of the real biosensor should be built [7, 8]. Modelling of a biosensor with a perforated membrane has been already performed by Schulmeister and Pfeiffer [9]. The proposed one-dimensional-in-space (1-D) mathematical model does not take into consideration the geometry of the membrane perforation and includes effective diffusion coefficients. Authors of the 1-D model have recognized that "its quantitative value is limited" [9].

Recently, a two-dimensional-in-space (2-D) mathematical model taking into consideration the perforation geometry has been proposed [10, 11]. However, a simulation of the biosensor action based on the 2-D model is much more time-consuming than a simulation based on the corresponding 1-D model. This is especially important when investigating numerically peculiarities of the biosensor response in wide ranges of catalytical and geometrical parameters. The multifold numerical simulation of the biosensor response based on the 1-D model is much more efficient than the simulation based on the corresponding 2-D model.

In this paper, we investigate the conditions at which the 1-D mathematical model can be applied to simulate accurately the biosensor action. The accuracy of the biosensor response simulated by using 1-D model was evaluated by the response simulated with the corresponding 2-D model. Additionally, this paper presents a procedure for numerical evaluation of the effective diffusion coefficient used in 1-D model. For a certain biosensor, the effective diffusion coefficient can be efficiently calculated having the response simulated with the corresponding 2-D model. The numerically calculated effective diffusion coefficient was compared with the corresponding coefficient derived analytically [12–14]. The numerical simulation was carried out using the finite difference technique [15].

## 2 Mathematical model

The biosensor operation is based on the enzymatic reaction and the mass transport by diffusion of substances. We consider an enzyme-catalysed reaction schematically expressed as follows:

$$\mathrm{E} + \mathrm{S} \rightleftarrows \mathrm{E\,S} \rightarrow \mathrm{E} + \mathrm{P}.$$

In this scheme the substrate (S) combines reversibly with the enzyme (E) to form a complex (ES). The complex then dissociates into a product (P) and the enzyme is regenerated [1, 2]. At the electrode surface the reaction product is involved into an electrochemical reaction where some electrons are released. The electrical signal is then amplified and presented to end-user. In the case of amperometry, the biosensor current is proportional to the concentration of the substrate (target analyte).

Assuming the quasi steady state approximation, the concentration of the intermediate complex (ES) does not change and may be neglected when simulating the biochemical behaviour of biosensors [2, 16]. At these conditions, the rate of the enzymatic reaction is usually described by the Michaelis-Menten equation,

$$R(S) = \frac{V_{max} S}{K_M + S}, \tag{1}$$

where $V_{max}$ is the maximal rate of the enzymatic reaction, $K_M$ is the Michaelis constant, $S$ is the concentration of the substrate and $R(S)$ represents the reaction rate as a function of the substrate concentration [16, 17].

A practical biosensor contains a multilayer enzyme membrane. The electrode acting as a transducer of the biosensor is covered by a selective membrane, following a layer of immobilized enzyme and an outer membrane [2, 9]. Fig. 1 presents such biosensor schematically.

For the biosensor shown in Fig. 1, one and two-dimensional-in-space mathematical models are known [9, 10]. The 2-D model takes into consideration the geometry of perforation, and therefore describes the biosensor in more detail. In the 1-D model the perforated membrane is modelled by a homogeneous layer with an appropriate effective diffusion coefficient and the reaction rate.

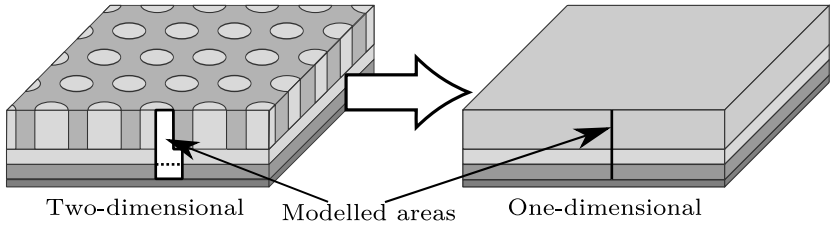


Fig. 1. Principal structures of a practical biosensor with a perforated membrane and of the corresponding simplified biosensor in which the perforated membrane is treated as a homogeneous medium. Figure is not to scale.

### 2.1 Two-dimensional-in-space model

When modelling a practical biosensor, the holes in the perforated membrane were modelled by right cylinders of uniform diameter and spacing, forming a regular hexagonal pattern. The entire biosensor may be divided into equal hexagonal prisms with regular hexagonal bases. For simplicity, it is reasonable to consider a circle whose area equals to that of the hexagon and to regard one of the cylinders as a unit cell of the biosensor. Due to the symmetry of the unit cell, only a half of the transverse section of the unit cell is considered in 2-D mathematical model formulated in cylindrical coordinates [10, 11].

Fig. 2(a) shows the profile of the unit of the biosensor, where $\Omega_1$ represents the selective membrane, $\Omega_2$ corresponds to the enzyme region, $\Omega_3$ stands for the buffer solution, and $\Omega_4$ represents an impermeable carrier of the perforated membrane,

$$\begin{aligned} &\Omega_1 = (0, r_2) \times (0, z_1), \qquad &&\Omega_2 = (0, r_2) \times (z_1, z_3) \setminus \overline{\Omega}_4, \\ &\Omega_3 = (0, r_1) \times (z_3, z_4), \qquad &&\Omega_4 = (r_1, r_2) \times (z_2, z_4), \end{aligned} \tag{2}$$

here and below $\overline{\Omega}_i$ is the closed region corresponding to open region $\Omega_i$, $i = 1, 2, 3, 4$.

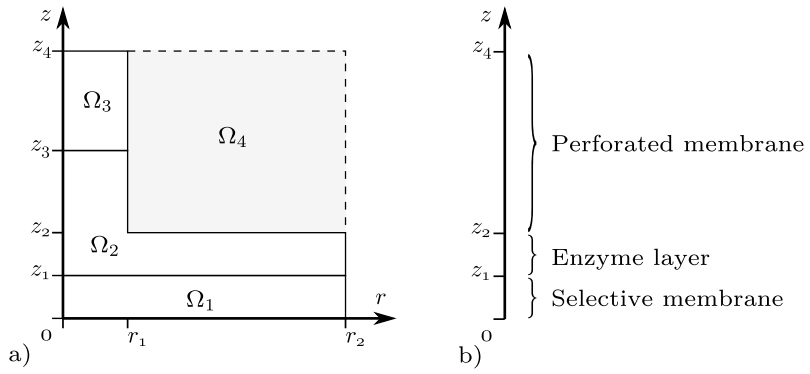


Fig. 2. The profiles of the unit cell in 1-D (a) and 2-D (b) domain. Figure is not to scale.

In Fig. 2, $r_2$ is the radius of the base of the unit cell, $r_1$ is the radius of the holes, $z_1$ stands for the thickness of the selective membrane, $z_2 - z_1$ is the thickness of the basic enzyme layer, $z_4 - z_2$ is the thickness of the perforated membrane. We assume that the holes can be fully or partially filled with the enzyme, $z_3$ stands for the level of filling the holes.

In the region $\Omega_1$ corresponding to the selective membrane, only the mass transport by diffusion of the product takes place,

$$\frac{\partial P_1}{\partial t} = D_1 \Delta P_1, \quad (r, z) \in \Omega_1, \;\; t > 0, \tag{3}$$

where $P_1 = P_1(r, z, t)$ is the product concentration in $\overline{\Omega}_1$, $D_1$ is the diffusion coefficient of the product in the selective membrane, and $\Delta$ is the Laplace operator in cylindrical coordinates [15]. There is no substrate in $\Omega_1$.

In the enzyme region $\Omega_2$, the enzymatic reaction and the diffusion of the substrate and the product take place. The dynamics of the concentrations is described by the reaction-diffusion equations ($t > 0$),

$$\frac{\partial S_2}{\partial t} = D_2 \Delta S_2 - R(S_2), \quad \frac{\partial P_2}{\partial t} = D_2 \Delta P_2 + R(S_2), \quad (r, z) \in \Omega_2, \tag{4}$$

where $S_2 = S_2(r,z,t)$ and $P_2 = P_2(r,z,t)$ are the substrate and product concentrations in $\overline{\Omega}_2$, $D_2$ is the diffusion coefficient of the substrate and the product in the enzyme. Although, the diffusion coefficients for the substrate and product can be different, in this work for simplicity we use identical coefficients for both species.

In the region $\Omega_3$, the mass transport of both species by diffusion takes place,

$$\frac{\partial S_3}{\partial t} = D_3 \Delta S_3, \quad \frac{\partial P_3}{\partial t} = D_3 \Delta P_3, \quad (r,z) \in \Omega_3, \;\; t > 0, \tag{5}$$

where $S_3 = S_3(r,z,t)$ and $P_3 = P_3(r,z,t)$ are the substrate and product concentrations in $\overline{\Omega}_3$, and $D_3$ is the diffusion coefficient of these substances in the diffusion region.

Equations (3), (4) and (5) describe the concentrations of the substrate and product in the open areas $\Omega_1$, $\Omega_2$ and $\Omega_3$. In addition to these equations, the initial, boundary and matching conditions are required.

For further convenience, we introduce the following symbols:

$$\begin{aligned}
&\Gamma_0 = [0, r_2] \times \{0\}, \\
&\Gamma_i = \overline{\Omega}_i \cap \overline{\Omega}_{i+1}, \quad i = 1, 2, \\
&\Gamma_3 = [0, r_1] \times \{z_4\}, \\
&\Gamma_{nl} = \left(\overline{\Omega}_1 \cup \overline{\Omega}_2 \cup \overline{\Omega}_3\right) \setminus (\Omega_1 \cup \Omega_2 \cup \Omega_3) \setminus (\Gamma_0 \cup \Gamma_1 \cup \Gamma_2 \cup \Gamma_3).
\end{aligned} \tag{6}$$

The non-leakage conditions were applied for the boundaries on which the species touches the impermeable carrier of the perforated or selective membrane and for the boundaries corresponding the symmetry axis of the modelled cell as well as the perimeter of it,

$$\begin{aligned}
&D_i \frac{\partial S_i}{\partial n}\bigg|_{\overline{\Omega}_i \cap \Gamma_{nl}} = 0, \quad i = 2, 3, \\
&D_i \frac{\partial P_i}{\partial n}\bigg|_{\overline{\Omega}_i \cap \Gamma_{nl}} = 0, \quad i = 1, 2, 3, \\
&D_2 \frac{\partial S_2}{\partial n}\bigg|_{\Gamma_1} = 0,
\end{aligned} \tag{7}$$

where $n$ stands for the normal direction.

The matching conditions were used for the boundaries between adjacent regions with the different diffusivities,

$$\begin{aligned}
&S_2 = S_3, \;\; (r,z) \in \Gamma_2, \qquad D_2 \left.\frac{\partial S_2}{\partial n}\right|_{\Gamma_2} = D_3 \left.\frac{\partial S_3}{\partial n}\right|_{\Gamma_2}; \\
&P_i = P_{i+1}, \;\; (r,z) \in \Gamma_i, \qquad D_i \left.\frac{\partial P_i}{\partial n}\right|_{\Gamma_i} = D_{i+1} \left.\frac{\partial P_{i+1}}{\partial n}\right|_{\Gamma_i}, \quad i = 1, 2.
\end{aligned} \tag{8}$$

The conditions for the external boundary of the biosensor and for the surface of the electrode were defined by the following equations:

$$\begin{aligned}
&S_3(r, z_4, t) = S_0, \;\; P_3(r, z_4, t) = 0, \quad r \in [0, r_1], \\
&P_1(r, 0, t) = 0, \quad r \in [0, r_2],
\end{aligned} \tag{9}$$

where $S_0$ is the concentration of the substrate in the bulk solution.

The simulation of the biosensor action starts in the state where no substrate appears inside the biosensor, but the external surface of the biosensor already touches the analyte. This state is defined by initial conditions ($t = 0$) of the biosensor operation [10],

$$\begin{aligned} &P_i = 0, \quad (r,z) \in \overline{\Omega}_i, \;\; i = 1,2,3, \\ &S_i = 0, \quad (r,z) \in \overline{\Omega}_i \setminus \Gamma_3, \;\; i = 2,3, \\ &S_3 = S_0, \quad (r,z) \in \Gamma_3. \end{aligned} \tag{10}$$

The current density of the amperometric biosensor is proportional to the concentration gradient of the reaction product at the electrode surface,

$$\begin{aligned} i(t) &= n_e F D_1 \frac{1}{\pi r_2^2} \int_0^{2\pi} \int_0^{r_2} \left. \frac{\partial P_1}{\partial z} \right|_{z=0} r \,\mathrm{d}r \,\mathrm{d}\varphi, \\ &= n_e F D_1 \frac{2}{r_2^2} \int_0^{r_2} \left. \frac{\partial P_1}{\partial z} \right|_{z=0} r \,\mathrm{d}r, \end{aligned} \tag{11}$$

where $i(t)$ is the density of the current at time $t$, $\varphi$ is the third cylindrical coordinate, $n_e$ is a number of electrons emitted in the electrochemical reaction, and $F$ is the Faraday constant [10, 16].

Often the end-user of the biosensor is interested only in the final result – the stationary current,

$$I = \lim_{t \to \infty} i(t), \tag{12}$$

where $I$ is the density of steady state current.

### 2.2 One-dimensional-in-space model

Assuming the perforated membrane as the periodic medium, the homogenization process can be applied to it [18]. According to this approach, the perforated membrane is replaced by a homogeneous medium with the properties similar to the properties of the perforated membrane. This makes possible to describe the biosensor operation in 1-D space [9, 19]. In this section, we define a 1-D model that corresponds to the 2-D model (2)–(12).

The 1-D mathematical model contains three governing equations, each of which corresponds to a layer shown in Fig. 2(b). The diffusion of the product that takes place in the selective membrane is defined by the equation

$$\frac{\partial P_1^*}{\partial t} = D_1 \Delta P_1^*, \quad z \in (0, z_1), \;\; t > 0, \tag{13}$$

where $P_1^* = P_1^*(z,t)$ is the product concentration in the selective membrane, $\Delta$ is the Laplace operator formulated in the one-dimensional Cartesian coordinate system.

In the one-dimensional modelling, the enzyme region covers only the interval in which the mass transport and the enzyme reaction are described by the following equations ($t > 0$):

$$\frac{\partial S_2^*}{\partial t} = D_2 \Delta S_2^* - R(S_2^*), \quad \frac{\partial P_2^*}{\partial t} = D_2 \Delta P_2^* + R(S_2^*), \quad z \in (z_1, z_2), \tag{14}$$

where $S_2^* = S_2^*(z,t)$ and $P_2^* = P_2^*(z,t)$ are the concentrations of the substrate the product in the enzyme layer, respectively.

Since the perforated membrane is a non-homogeneous media, a homogenization process have to be applied to it [9,18]. The dynamics of the concentrations of the substrate and product in the homogenized perforated membrane as follows ($t > 0$):

$$\frac{\partial S_3^*}{\partial t} = D_3^* \Delta S_3^* - \gamma R(S_3^*), \quad \frac{\partial P_3^*}{\partial t} = D_3^* \Delta P_3^* + \gamma R(S_3^*), \quad z \in (z_2, z_4), \tag{15}$$

where $S_3^* = S_3^*(z,t)$ and $P_3^* = P_3^*(z,t)$ are the concentrations of the substrate and the product in the layer $[z_2, z_4]$, $D_3^*$ is the effective diffusion coefficient of the substrate and product in the homogenized perforated membrane, $\gamma$ is the correction coefficient for the rate of the enzymatic reaction.

As in the 2-D model, the matching conditions were defined for the common points of the adjacent intervals,

$$\begin{aligned}
&D_1 \left.\frac{\partial P_1^*}{\partial z}\right|_{z=z_1} = D_2 \left.\frac{\partial P_2^*}{\partial z}\right|_{z=z_1}, \qquad P_1^*(z_1,t) = P_2^*(z_1,t), \\
&D_2 \left.\frac{\partial P_2^*}{\partial z}\right|_{z=z_2} = D_3^* \left.\frac{\partial P_3^*}{\partial z}\right|_{z=z_2}, \qquad P_2^*(z_2,t) = P_3^*(z_2,t), \\
&D_2 \left.\frac{\partial S_2^*}{\partial z}\right|_{z=z_2} = D_3^* \left.\frac{\partial S_3^*}{\partial z}\right|_{z=z_2}, \qquad S_2^*(z_2,t) = S_3^*(z_2,t).
\end{aligned} \tag{16}$$

The rest boundary conditions are also very similar to that used in the 2-D model,

$$P_1^*(0,t) = 0, \quad D_2 \left.\frac{\partial S_2^*}{\partial z}\right|_{z=z_1} = 0, \quad S_3^*(z_4,t) = S_0, \quad P_3^*(z_4,t) = 0. \tag{17}$$

The initial conditions were defined as follows:

$$\begin{aligned}
&P_1^*(z,0) = 0, \quad z \in [0, z_1], \\
&S_2^*(z,0) = P_2^*(z,0) = 0, \quad z \in [z_1, z_2], \\
&S_3^*(z,0) = P_3^*(z,0) = 0, \quad z \in [z_2, z_4), \\
&S_3^*(z_4,0) = S_0, \quad P_3^*(z_4,0) = 0.
\end{aligned} \tag{18}$$

The density of the current generated by the biosensor at the time $t$ is defined in the same way as in the 2-D model only rewritten for the 1-D Cartesian coordinate system,

$$i^*(t) = n_e F D_1 \left.\frac{\partial P_1^*}{\partial z}\right|_{z=0}. \tag{19}$$

Correspondingly, the density of the steady state current is defined as follows:

$$I^* = \lim_{t\to\infty} i^*(t). \tag{20}$$

### 2.3 Effective diffusion coefficient and reaction rate

In comparison with the 2-D model (3)–(5), (7)–(10), the 1-D model (13)–(18) of the biosensor action contains two additional parameters: the coefficient $D_3^*$ of the effective diffusion and the effectiveness coefficient $\gamma$ of the enzymatic reaction. These two parameters arose when applying the homogenization process to the perforated membrane [18,20]. The parameters have a limited physical sense [9].

According to the volume averaging approach [20], the correction coefficient $\gamma$ for the reaction rate can be calculated as the volume fraction of the enzyme in the entire perforated membrane (see Fig. 2),

$$\gamma = \frac{\pi r_1^2 (z_3 - z_2)}{\pi r_2^2 (z_4 - z_2)} = \alpha\beta, \tag{21}$$

where $\alpha$ stands for a perforation level, and $\beta$ is a level of filling the holes with the enzyme,

$$\alpha = \frac{\pi r_1^2}{\pi r_2^2} = \frac{r_1^2}{r_2^2}, \quad \beta = \frac{z_3 - z_2}{z_4 - z_2}. \tag{22}$$

The perforation level $\alpha$ can also be called as the volume fraction of holes in the perforated membrane, while filling level $\beta$ as the relative volume of the enzyme in the holes.

One of the most general restrictions for the effective diffusivity $D_3^*$ can be expressed as follows:

$$0 \le D_3^* \le \max(D_2, D_3). \tag{23}$$

The more precise evaluation of the diffusivity $D_3^*$ should take into consideration the geometry of the membrane perforation. The volume averaging approach can be also applied to evaluate the effective diffusivity $D_3^*$ [18, 20].

In the case when the material is a two-phase composite, the effective diffusion coefficient $d^*$ is considered as a function of the constituent diffusion coefficients ($d_1$ and $d_2$) and the volume fraction ($\upsilon$) [21, 22],

$$\frac{d_1 d_2}{\upsilon d_2 + (1-\upsilon) d_1} \le d^* \le \upsilon d_1 + (1-\upsilon) d_2, \tag{24}$$

where $d_i$ is the diffusion coefficient of the species in a phase $i$, $i = 1, 2$, and $\upsilon$ is the volume fraction of the species in the phase 1. Accordingly, the volume fraction of the species 2 equals $(1 - \upsilon)$.

The effective diffusion coefficient $d^*$ in a two-phase composite can be also evaluated by it's upper bound given in (24) and the tortuosity factor $\theta$ ($0 \le \theta \le 1$) [12, 14],

$$d^* = \theta\big(\upsilon d_1 + (1-\upsilon) d_2\big). \tag{25}$$

Very similar approach to the effective diffusion coefficient was applied in modelling of glucose diffusion through an isolated pancreatic islet of Langerhans [13].

When modelling holes of the perforated membrane by rights cylinders, the tortuosity of the holes equals approximately to unity, $\theta \approx 1$. Consequently, the effective diffusion coefficient $D_h^*$ inside the holes can be calculated as follows:

$$D_h^* = \beta D_2 + (1-\beta) D_3, \tag{26}$$

where $\beta$ is the volume fraction of the enzyme inside the holes as defined in (22). Assuming zero diffusivity of both species in the insulator region $\Omega_4$ and the unity tortuosity of holes, we apply the formula (25) to the entire perforated membrane to calculate the effective diffusion coefficient $D_3^*$,

$$D_3^* = \alpha D_h^* = \alpha\big(\beta D_2 + (1-\beta) D_3\big). \tag{27}$$

Although, the volume averaging approach is widely used, several cases are when the generally-accepted it gives incorrect results. The case of an impermeable aggregate is among them [23]. In such case, more precise modelling of a reaction-diffusion system requires additional parameters [24]. On the other hand, the 2-D model taking into consideration the geometry of the membrane perforation requires no correction coefficients.

In Section 4 we describe a procedure for numerical evaluation of the effective diffusion coefficient used in 1-D model. Applying this approach for a certain biosensor, the effective diffusion coefficient is calculated having the response simulated with the corresponding 2-D model.

## 3 Numerical simulation

Biosensors with selective and perforated membranes were modelled by non-stationary reaction-diffusion equations containing a non-linear term defining the enzymatic reaction. Analytical solutions for this type of equations are known only in very limited cases [17, 25]. Therefore, the initial boundary value problems were solved numerically by using finite difference technique [15, 26, 27].

A domain of the problem was discretized using a quasi-uniform grid. In the case of 2-D model, discretization was done using variable steps in time and space. The same approach was used in [10, 11]. In the case of 1-D model, a constant step $\tau = 0.001$ s was used for a time dimension. A space dimension of the 1-D model was discretized by using uniform grid for each interval of $[0, z_1]$, $[z_1, z_2]$ and $[z_2, z_4]$. In all simulations each of these intervals was divided into $200$ equal parts.

Applying the alternating direction method to 2-D model, a semi-implicit linear finite difference scheme has been built as a result of the difference approximation [10]. The system of linear algebraic equations was solved efficiently because of the tridiagonality of the system matrix.

The densities $I$ and $I^*$ of the steady state current are limits when $t \to \infty$. In numerical simulation, the stationary biosensor response time was assumed as the time

when the absolute current slope value falls below a given small value normalized with the current and time. In other words, the time needed to achieve a given dimensionless decay rate $\varepsilon$ was used, and the density $I_R$ of the steady state current was defined by

$$\begin{aligned} &I_R = i(T_R) \approx I, \quad T_R = \min_{i_j>0} \left\{ t_j : \ \frac{i_j - i_{j-1}}{\tau} \times \frac{t_j}{i_j} < \varepsilon \right\}, \\ &t_j = \tau j, \quad i_j = i(t_j), \quad j = 1, 2, \ldots, \end{aligned} \tag{28}$$

where $\tau$ stands for the size of time step, and $T_R$ is an approximate time at which the steady state is reached. In calculation, $\varepsilon = 0.01$ was used.

The response time $T_R$ is highly sensitive to the decay rate $\varepsilon$, i.e. $T_R \to \infty$ when $\varepsilon \to 0$. Because of this, we use a less sensitive part of the steady state time by introducing the resultant relative output signal function $\overline{i}(t)$,

$$\overline{i}(t) = \frac{I_R - i(t)}{I_R}, \quad 0 \le \overline{i}(t) \le 1. \tag{29}$$

We use the half-time $T_{0.5}$ defined by $\overline{i}(T_{0.5}) = 0.5$. $T_{0.5}$ expresses the time at which the half of the steady state current is reached [10, 17]. In the case of the 1-D model the half-time of the stationary current $T^*_{0.5}$ is defined in the same way.

The numerical simulation was performed at different geometries of the membrane perforation and the level $\beta$ of filling the holes with the enzyme. The following values of the model parameters were constant in all the numerical experiments:

$$\begin{aligned} &D_1 = 1\ \mu\text{m}^2/\text{s}, \quad D_2 = 300\ \mu\text{m}^2/\text{s}, \quad D_3 = 600\ \mu\text{m}^2/\text{s}, \\ &r_2 = 1\ \mu\text{m}, \quad z_1 = 2\ \mu\text{m}, \quad z_2 = z_1 + 2\ \mu\text{m}, \quad z_4 = z_2 + 10\ \mu\text{m}, \\ &K_M = 100\ \mu\text{M}, \quad V_{max} = 10\ \mu\text{M/s}, \quad n_e = 2. \end{aligned} \tag{30}$$

## 4 Calculation of the effective diffusion coefficient

The coefficient $D_3^*$ is the effective diffusivity of the substrate and product in the homogenized perforated membrane. Assuming the 2-D model as the model where the perforated membrane is modelled precisely, the effective diffusion coefficient $D_3^*$ can be found by minimizing the difference between the responses of the 2-D and the corresponding 1-D models. We introduce the relative error $\eta$ of the steady state current calculated by using 1-D model,

$$\eta_I(D, S_0) = \frac{|I - I^*|}{I}, \tag{31}$$

where $D$ stands for a value of the effective diffusion coefficient $D_3^*$ used in numerical modelling, $S_0$ is the concentration of the substrate to be analyzed, $I$ is the density of the stationary current calculated by using 2-D model, and $I^*$ is the density of the stationary current calculated by using corresponding 1-D model. In definition (31), $I$ is assumed as the true value of the biosensor current density, while $I^*$ – as the approximate one.

The relative error $\eta_I$ depends on the value of the effective diffusion coefficient $D_3^*$ used in the 1-D model and the catalytical as well as the geometrical parameters of the modelled biosensor. Values of all the parameters of the 1-D model excluding only $D_3^*$ can be derived directly from the corresponding 2-D model. For a concrete substrate concentration $S_0$, the effective diffusion coefficient $D_3^*$ can be expressed as a value minimizing the relative error $\eta_I$,

$$D_3^*(S_0) = \arg\min_D \eta_I(D, S_0), \quad 0 \leq D \leq \max(D_2, D_3), \tag{32}$$

where the upper value of $D$ comes from (23).

The minimization (32) can be achieved by changing $D$ and solving the 1-D model of the biosensor action using different values $D$ of $D_3^*$. In order to find the value of $D_3^*$ in the efficient way, the following procedure was introduced.

Let $E^*$ be an ordered sequence of triplets $\langle D_{3,i}^*, I_i^*, T_{0.5,i}^* \rangle$, where $I_i^*$ is the density of the simulated stationary current, $T_{0.5,i}^*$ is the half-time of the steady state, and $D_{3,i}^*$ denotes the averaged diffusion coefficient used in the simulation, $i = 1, 2, \ldots$. Each triplet in the sequence $E^*$ couples the parameters characterizing a concrete simulation of the biosensor action by using 1-D model. The half-time $T_{0.5,i}^*$ of the steady state response stands for the dynamics of the biosensor action. The order in this sequence is preserved according to the following rule: $D_{3,i}^* \geq D_{3,i+1}^*, \forall i \geq 1$. The procedure of calculation of $D_3^*$ is defined by the following steps:

1. Simulate the operation of a particular biosensor using the 2-D model. The steady state current density $I$ and half-time $T_{0.5}$ of the steady state are results of this simulation to be used in the next steps. Go to step 2.

2. Perform a preliminary variation of the effective diffusion coefficient $D_3^*$. The biosensor responses are simulated by using the 1-D model changing values of $D_3^* \in [0, \max(D_2, D_3)]$. The simulation results are appended to the sequence $E^*$. Let $M$ denote the number of elements in $E^*$. Go to step 3.

3. Construct a set of intervals $G = \{[D_{3,i+1}^*, D_{3,i}^*] \colon I_{i+1}^* \leq I \leq I_i^*$ or $I_{i+1}^* \geq I \geq I_i^*, i \geq 1\}$. If $G = \emptyset$ then go to step 4, otherwise go to step 6.

4. Find $m$ ($1 \leq m \leq M$) for which the difference $|I_m^* - I|$ is the minimal. If variation of the effective diffusion coefficient of the adjacent elements in the sequence $E^*$ is small enough, i.e. $(D_{3,m-1}^* - D_{3,m+1}^*)/D_{3,m}^* < \epsilon$, then stop the procedure with $D_{3,m}^*$ as the output. Otherwise, go to step 5.

5. Simulate two more responses of the biosensor at $D_3^* = (D_{3,m-1}^* + D_{3,m}^*)/2$ and $D_3^* = (D_{3,m}^* + D_{3,m+1}^*)/2$, where $m$ comes from step 4. Append the corresponding two triplets to the sequence $E^*$ and go to step 3.

6. For each interval from the set $G$ produced in step 3, apply the method of chords (secants [27]) to find a number of values of $D_3^*$ minimizing (32). Between them, find $k$-th for which the corresponding difference $|T_{0.5} - T_{0.5,k}^*|$ is minimal. The output of the procedure is $D_{3,k}^*$.

In step 2, the preliminary variation of the effective diffusion coefficient $D_3^*$ can be done in a number of different ways. In this work, it was achieved by simulating the biosensor action by using the 1-D model at the values of $D_3^*$ chosen as follows:

$$D_{3,j}^* = \begin{cases} \max(D_2, D_3), & j = 1; \\ \frac{D_{3,j-1}^*}{2}, & j = 2, \ldots, N. \end{cases} \tag{33}$$

This sequence is constructed in the way to cover the entire domain of $D_3^*$ ($0 < D_3^* \leq \max(D_2, D_3)$) and to find a smaller subdomain in which the value minimizing the error $\eta_I$ exists. The result of each simulation is appended to the sequence $E^*$. The preliminary variation is performed until the stationary current density $I_j^*$ starts to decrease and becomes smaller than $I$.

An application of the proposed procedure is illustrated in Fig. 3. The figure shows values of the effective diffusion coefficient $D_3^*$ used in 1-D simulations and the corresponding steady state current densities. All the simulations were performed at $r_1$ = 100 nm, $r_2 = 10\, r_1$, $z_3 = z_4$, $S_0$ = 3.3 mM and values defined in (30).

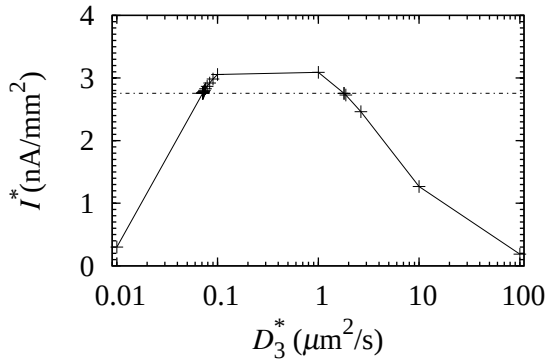


Fig. 3. The stationary current density $I^*$ versus the effective diffusion coefficient $D_3^*$ obtained by applying the procedure. The dashed line shows the stationary current density $I$ obtained by using 2-D model, $r_1$ = 100 nm ($\alpha = 0.01$), $z_3 = z_4$ ($\beta = 1$), $S_0$ = 3.3 mM, values of all other parameters are as defined in (30).

Using 2-D simulation, we obtained the density $I$ of the stationary current of $2.76$ nA/mm$^2$. A half of the steady state current was reached at $4.4$ s, $T_{0.5}$ = $4.4$ s. In Fig. 3, the horizontal dashed line shows the stationary current density $I$ calculated by using 2-D model. This line crosses the curve drawn through values of the effective diffusion coefficient. Two crossing points represent the values of $D_3^*$ for which the relative error $\eta_I$ equals to $0$, i.e. at two values (0.07 and 1.8 $\mu$m$^2$/s) of $D_3^*$ the 1-D simulation produces the stationary current identical to that calculated by using 2-D model, $I^* = I$. Having two values of $D_3^*$ at which $\eta_I = 0$, we choose only one of them under consideration of the response time. Applying $D_3^* = 0.07$ $\mu$m$^2$/s to 1-D simulation, the half-time $T_{0.5}^*$ was found to be $191$ s, while at $D_3^* = 1.8$ $\mu$m$^2$/s the time $T_{0.5}^*$ equals

13.4 s. Since $|4.4 - 191| > |4.4 - 13.4|$, the resulting effective diffusion coefficient $D_3^*$ equals approximately 1.8 $\mu$m$^2$/s.

At this concrete geometry of the perforation ($r_1$ = $0.1r_2$, $\alpha = 0.01$) and the level of filling the holes with the enzyme ($z_3 = z_4$, $\beta = 1$), the effective diffusion coefficient $D_3^*$ can be independently calculated from (27), $D_3^*$ = 0.01 * 300 = 3 ($\mu$m$^2$/s). This value of $D_3^*$ notably differs from that (1.8 $\mu$m$^2$/s) calculated by applying the procedure presented in this section. Below we investigate this effect in details.

## 5 Results and discussion

In order to determine conditions under which the 1-D model (13)–(18) may be used for accurate prediction of the biosensor response, a modelling error was investigated at different geometries of the membrane perforation and catalytical parameters of the biosensor. The modelling error was estimated by comparing the biosensor response simulated by using 1-D model with the response obtained by using the corresponding 2-D model.

A concrete practical biosensor is usually used for analysing the substrate of different concentrations. Because of this, it is important to evaluate the modelling error for a wide range of the substrate concentrations. An application of the 2-D model for calculation of the "true" biosensor response is an essential feature of the procedure to be used for determination of the effective diffusion coefficient $D_3^*$. The simulation of the biosensor response supposes a particular concentration of the substrate. If the substrate concentration effects the modelling error then it is important to determine the concentration to be used in the procedure when calculating a value of $D_3^*$. On the other hand, having a value of $D_3^*$, it is important to determine an interval of substrate concentrations for which the value of $D_3^*$ can be applied for accurate prediction of the response.

We introduce a relative error of 1-D modelling as follows:

$$\eta_S(S_D, S_V) = \eta_I\big(D_3^*(S_D), S_V\big), \tag{34}$$

where $D_3^*$ is the effective diffusion coefficient introduced by (32), $S_D$ is the substrate concentration used in 2-D simulation when calculating the effective diffusion coefficient, $S_V$ is the substrate concentration used in 1-D simulation. $\eta_S$ can be called as a 1-D modelling error arose because of an application of $D_3^*$ for the prediction of the biosensor response at the substrate concentration $S_V$.

The coefficient $D_3^*$ minimizes the relative error $\eta_I$ for a particular substrate concentration $S_D$. $\eta_S$ evaluates the error for any concentration ($S_V$) of the substrate. In order to cover the entire range of the practical concentrations, the error $\eta_S$ was evaluated for $\forall S_D \in \hat{S}$ and $\forall S_V \in \hat{S}$, where $\hat{S} = \{2^k \times 100\,\text{nM},\ k = 0, 1, \ldots, 20\}$.

The 1-D model was validated for different values of the membrane perforation level $\alpha$ (radius $r_1$ of the holes) and of the level $\beta$ of filling the holes with the enzyme. The level $\alpha$ was varied by changing the radius $r_1$ of the perforation holes, while the level $\beta$ was varied by changing $z_3$ from $z_2$ to $z_4$. Values of all other parameters of the biosensor action were kept constant.

### 5.1 The effect of the level of filling the holes

In order to investigate the dependence of the relative error $\eta_I$ on the level $\beta$ of filing the holes of the perforated membrane with the enzyme, the biosensor response was simulated at the following three values of $\beta$: 0 ($z_3 = z_2$) when the holes were fully filled with the buffer solution (no enzyme in the holes), 0.5 ($z_3 = (z_2 + z_4)/2$) when the holes were half-filled with the enzyme, and 1 ($z_3 = z_4$) when holes were fully filled with the enzyme. Calculated values of the relative error $\eta_S$ are depicted in the Fig. 4.

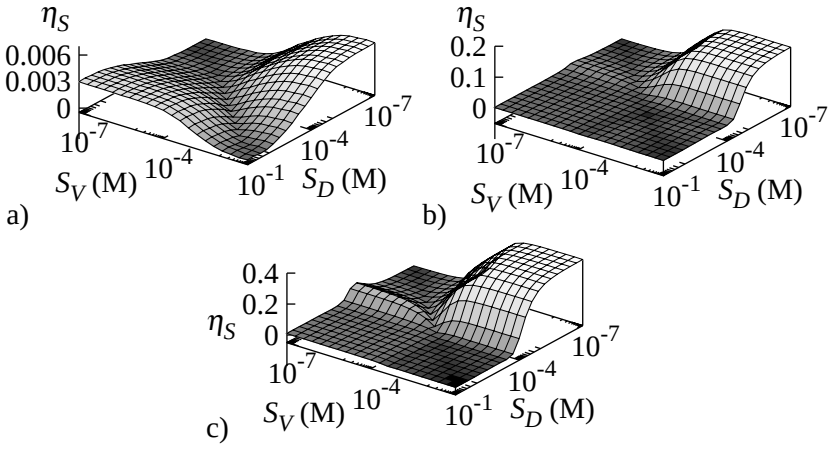


Fig. 4. The relative error $\eta_S$ at three levels ($\beta$) of the enzyme filling: 0 (a), 0.5 (b) and 1 (c); $\alpha = 0.01$, values of all other parameters are as defined in (30).

The smallest relative errors were achieved in the case when there was no enzyme in the holes (Fig. 4(a)). In this case, $\eta_S$ was less than $0.6\ \%$. When the level of the enzyme raises, a preciseness of the 1-D model decreases. In the case when $\beta = 1$ ($z_3 = z_4$) the relative error of the 1-D model reaches $37\ \%$ (Fig. 4(c)). When the holes were half-filled with the enzyme, the modelling error was less than $15\%$ (Fig. 4(b)).

Fig. 4 also shows the dependence of the error $\eta_S$ on the substrate concentrations $S_D$ (used in 2-D simulation when calculating the effective diffusion coefficient $D_3^*$) and $S_V$ (used in 1-D simulation). One can see in Fig. 4 that the relative error $\eta_S$ is usually smaller when 1-D model is applied for the substrate concentration $S_V$ smaller than that ($S_D$) used in 2-D simulation for evaluation of $D_3^*$. Consequently, the substrate concentration used to find the effective diffusion coefficient should be chosen larger than concentrations for which the 1-D model will be applied.

Fig. 5 shows the relative errors in the same three cases of the enzyme filling, but applying two different approaches for calculation of the effective diffusion coefficient $D_3^*$. The procedure defined in the previous section was the first approach (curves 1–3), while the formula (27) was the second one (curves 4–6). When applying the procedure, a practically maximal concentration ($S_0$ = $S_D = 0.1$ M) of the substrate was used. As one

can see in Fig. 5, the relative errors are notable less for $D_3^*$ calculated by the procedure rather than calculated analytically by (27). This property is especially bright when 1-D model is applied at high concentrations of the substrate when the corresponding errors differs in orders of magnitude.

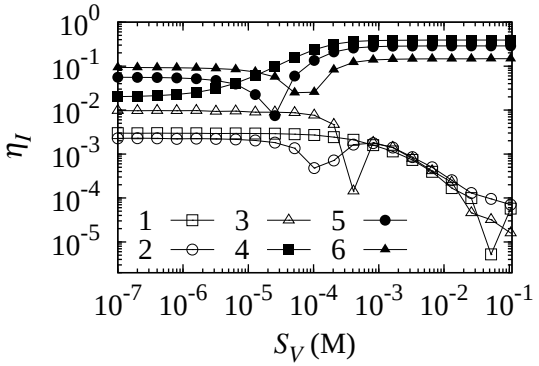


Fig. 5. The relative error $\eta_I$ at three levels ($\beta$) of the enzyme filling: 0 (1, 4), 0.5 (2, 5) and 1 (3, 6). The effective diffusion coefficient $D_3^*$ was calculated by applying the procedure at $S_D = 0.1$ M (1–3) as well as by applying formula (27) (4–6).

### 5.2 The effect of the perforation level

In order to investigate the effect of the relative radius $\alpha$ of the holes of the perforated membrane, the biosensor response was simulated at the following three values of $\alpha$: $10^{-3}$ ($r_1 = 10^{-\frac{3}{2}} r_2$), $10^{-2}$ ($r_1 = 10^{-1} r_2$) and $10^{-1}$ ($r_1 = 10^{-\frac{1}{2}} r_2$). The holes of the perforated membrane were assumed as fully filled with the enzyme, i.e. $\beta = 1$, $z_3 = z_4$. Calculated values of the relative error $\eta_S$ are depicted in Fig. 6.

One can see in Fig. 6 how the size of the holes influences the preciseness of the 1-D model. The maximal relative error $\eta_S$ decreases when the relative radius of the holes increases. In the case when the holes take only $0.1\%$ of the overall area of the membrane surface (Fig. 6(a)), the maximal values of $\eta_S$ exceed even $540$ %. In the case when the area of the holes is $10$ % of the overall area (Fig. 6(c)), the relative errors are less than $0.3$ %. In the case of $\alpha = 1$ ($r_1 = r_2$), the perforated membrane becomes so opened that it disappears at all, and the biosensor becomes a sandwich-like multilayer biosensor [2, 3, 17]. So, it is naturally that the error $\eta_S$ decreases with an increase in the level $\alpha$. Fig. 6 also approves the previous decision that the substrate concentration used to find the effective diffusion coefficient should be larger than concentrations for which the 1-D model will be applied.

Fig. 7 compares the relative errors for two different approaches used for calculation of the effective diffusion coefficient $D_3^*$. When applying the procedure (curves 1–3), the substrate concentration $S_0$ of $0.1$ M was used. As one can see in Fig. 7 that in the cases of relatively high perforation levels the relative errors are notable less for $D_3^*$ calculated

by the procedure rather than calculated analytically by (27) (curves 2, 3, 5 and 6). In the case of very low values of $\alpha$ (curves 1, 4), the errors are relatively high and practically does not depend on the approach of $D_3^*$ calculation.

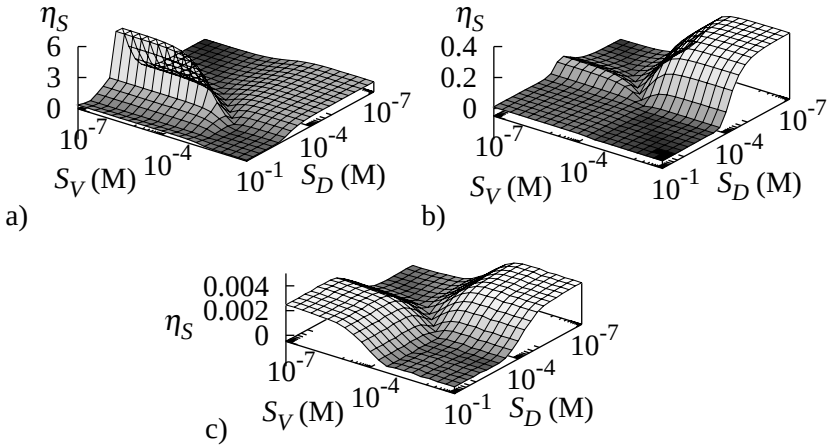


Fig. 6. The relative error $\eta_S$ at three levels ($\alpha$) of the membrane perforation: $10^{-3}$ (a), $10^{-2}$ (b) and $10^{-1}$ (c); $\beta = 1$, $V_{max}$ = 100 nM/s, values of all other parameters are as defined in (30).

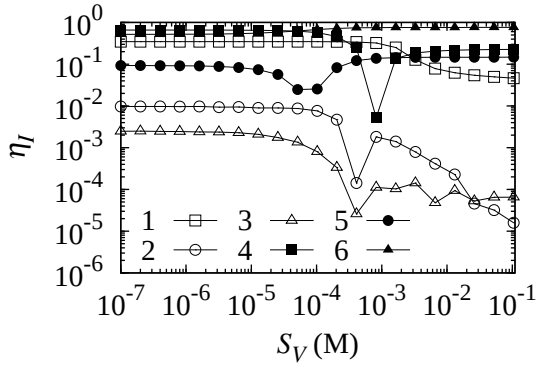


Fig. 7. The relative error $\eta_I$ at three levels ($\alpha$) of the membrane perforation: $10^{-3}$ (1, 4), $10^{-2}$ (2, 5) and $10^{-1}$ (3, 6); The effective diffusion coefficient $D_3^*$ was calculated by applying the procedure at the concentration $S_D = 0.1$ M (1–3) as well as by applying formula (27) (4–6).

## 6 Conclusions

The one-dimensional-in-space model (13)–(18) can be used to moderate simulation of the operation of the biosensor with the perforated membrane. The preciseness of this model depends on the geometry of the membrane perforation as well as on the level of filling the holes with the enzyme. The relative error of the 1-D modelling decreases with a decrease in the level of the enzyme in the holes of the perforated membrane (Fig. 4). The size of the holes has inverse influence to the modelling preciseness (Fig. 6).

The two-dimensional-in-space model (3)–(5), (7)–(10) of the biosensor with the perforated membrane can be used in order to find the value for the effective diffusion coefficient for the following usage in 1-D simulation. To decrease the modelling error, the substrate concentration used in the calculation of the effective diffusion coefficient should be chosen larger than concentrations for which the 1-D model will be applied.

The 1-D model is especially an inaccurate when the holes of the perforated membrane are very small (Figs. 6 and 7). In such cases the 2-D model should be used for an accurate prediction of the biosensor response.

## Acknowledgments

The authors express sincere gratitude to prof. Feliksas Ivanauskas and prof. Juozas Kulys for valuable discussions and their contribution into mathematical modelling of biosensors.

## References

1. A. P. F. Turner, I. Karube, G. S. Wilson, *Biosensors: Fundamentals and Applications*, Oxford University Press, Oxford, 1987.

2. F. Scheller, F. Schubert, *Biosensors*, Vol. 7, Elsevier, Amsterdam, 1992.

3. U. Wollenberger, F. Lisdat, F. W. Scheller, *Frontiers in Biosensorics 2, Practical Applications*, Birkhauser Verlag, Basel, 1997.

4. B. D. Malhotra, A. Chaubey, Biosensors for clinical diagnostics industry, *Sensor. Actuat. B-Chem.*, **91**, pp. 117–127, 2003.

5. D. Yu, B. Blankert, J.-C. Viré, J.-M. Kauffmann, Biosensors in drug discovery and drug analysis, *Anal. Lett.*, **38**, pp. 1687–1701, 2005.

6. H. Nakamura, I. Karube, Current research activity in biosensors, *Anal. Bioanal. Chem.*, **377**, pp. 446–468, 2003.

7. C. Amatore, A. Oleinick, I. Svir, N. da Mota, L. Thouin, Theoretical modeling and optimization of the detection performance: a new concept for electrochemical detection of proteins in microfluidic channels, *Nonlinear Anal. Model. Control*, **11**, pp. 345–365, 2006.

8. I. Stamatin, C. Berlic, A. Vaseashta, On the computer-aided modelling of analyte-receptor interactions for an efficient sensor design, *Thin Solid Films*, **495**, pp. 312–315, 2006.

9. T. Schulmeister, D. Pfeiffer, Mathematical modelling of amperometric enzyme electrodes with perforated membranes, *Biosens. Bioelectron.*, **8**, pp. 75–79, 1993.

10. R. Baronas, J. Kulys, F. Ivanauskas, Computational modelling of biosensors with perforated and selective membranes, *J. Math. Chem.*, **39**(2), pp. 345–362, 2006.

11. R. Baronas, Numerical simulation of biochemical behaviour of biosensors with perforated membrane, in: *Proc. 21st European Conference on Modelling and Simulation ECMS 2007*, I. Zelinka, Z. Oplatkova, A. Orsoni (Eds.), pp. 214–217, 2007.

12. E. J. Garboczi, Permeability, diffusivity and microstructural parameters: a critical review, *Cem. Concr. Res.*, **20**(4), pp. 591–601, 1990.

13. R. Bertram, M. Pernarowski, Glucose diffusion in pancreatic islets of Langerhans, *Biophys. J.*, **74**(4), pp. 1722–1731, 1998.

14. Y. Xi, Z. P. Bazant, Modeling chloride penetration in saturated concrete, *J. Mater. Civil. Eng.*, **11**(1), pp. 58–65, 1999.

15. A. A. Samarskii, *The Theory of Difference Schemes*, Marcel Dekker, New York-Basel, 2001.

16. A. Cornish-Bowden, *Fundamentals of Enzyme Kinetics*, 3rd ed., Portland Press, London, 2004.

17. T. Schulmeister, Mathematical modelling of the dynamic behaviour of amperometric enzyme electrodes, *Selective Electrode Rev.*, **12**, pp. 203–260, 1990.

18. N. S. Bakhvalov, G. P. Panasenko, *Homogenization: Averaging Processes in Periodic Media*, Kluwer Academic Publishers, Dordrecht, 1989.

19. R. Baronas, F. Ivanauskas, I. Kaunietis, V. Laurinavicius, Mathematical modeling of plate-gap biosensors with an outer porous membrane, *Sensors*, **6**(7), pp. 727–745, 2006.

20. S. Whitaker, *The Method of Volume Averaging*, Kluwer Academic Publishers, Boston, 1999.

21. L. Dormieux, E. Lemarchand, Homogenization approach of advection and diffusion in cracked porous material, *J. Eng. Mech. ASCE*, **127**(12), pp. 1267–1274, 2001.

22. D. W. Hobbs, Aggregate influence on chloride ion diffusion into concrete, *Cem. Concr. Res.*, **29**(12), pp. 1995–1998, 1999.

23. B. Jönson, H. Wennerström, P. G. Nilsson, P. Linse, Self-diffusion of small molecules in colloidal systems, *Colloid Polymer Sci.*, **264**(1), pp. 77–88, 1986.

24. J. R. Kalnin, E. A. Kotomin, J. Maier, Calculations of the effective diffusion coefficient for inhomogeneous media, *J. Phys. Chem. Solids*, **63**(3), pp. 449–456, 2002.

25. M. E. G. Lyons, T. Bannon, G. Hinds, S. Rebouillat, Reaction/diffusion with Michaelis-Menten kinetics in electroactive polymer films. Part 2. The transient amperometric response, *Analyst*, **123**(10), pp. 1947–1959, 1998.

26. D. Britz, *Digital Simulation in Electrochemistry*, 3rd ed., Springer-Verlag, Berlin, 2005.

27. J. Taler, P. Duda, *Solving Direct and Inverse Heat Conduction Problems*, Springer, Berlin, 2006.